DIRECT NUMERICAL SIMULATION OF PARTICLE-DRIVEN GRAVITY CURRENTS

Frieder Necker, Carlos Härtel, Leonhard Kleiser
Institute of Fluid Dynamics
ETH Zürich
ETH Zentrum, CH-8092 Zürich, Switzerland

Eckart Meiburg
Dept. Aerospace and Mechanical Engineering
University of Southern California
Los Angeles, CA 90089-1191, USA

ABSTRACT

Particle-driven gravity currents are examined by means of two-dimensional numerical simulations based on highly accurate integration schemes for the fluid-phase equations. Two different approaches are employed to describe the particulate phase, namely a Eulerian treatment and a Lagrangian particle-tracking technique. Good agreement is demonstrated between the two approaches for small particle Stokes numbers.

INTRODUCTION

Gravity currents, which form when a heavier fluid propagates into a lighter one, are frequently encountered both in the environment as well as in engineering applications (Simpson, 1997). Particle-driven gravity currents form a special class of these flows, as their density difference is caused by differential loading with suspended particles. Typical examples of such flows in geophysical applications are turbidity currents in oceans or lakes, and powder snow avalanches. To date, particle-driven gravity currents have mostly been investigated experimentally or on the basis of the shallow water equations (Bonnecaze *et al.*, 1993). The present research is intended to provide further insight into these flows by conducting two-dimensional (2D) direct numerical simulations (DNS).

PROBLEM FORMULATION

In fundamental research on gravity currents a prototype configuration is often considered, the so-called lock-exchange flow, in which a plane channel is filled with a fluid of constant density. A vertical splitter plate initially separates the particle-laden from the clear fluid (see Simpson, 1997). When the plate is withdrawn, a mutual intrusion flow develops. In the current report the lock-exchange configuration is studied by means of highly accurate DNS, i.e. simulations in which all relevant time and length scales in the flow are fully resolved. The disparity between the largest and smallest scales, which determines the numerical resolution required, depends on the ratio of buoyancy forces and viscous forces. This ratio will generally be expressed in terms of a Grashof number $Gr=(u_b h/\nu)^2$ here, where u_b is the buoyancy velocity based on the channel half-height h as the characteristic vertical length scale.

In our simulations the motion of the fluid phase is governed by the incompressible Navier-Stokes equations which are augmented by a forcing term that accounts for the effect of the particles on the fluid. The method used for the numerical integration of the NS equations employs a spatial discretization based on spectral and high-order compact finite-difference schemes, along with finite differences in time. A detailed description of the computational approach is given in Härtel *et al.* (1997). We focus on dilute concentrations here, for which particle-particle interactions can be neglected. Moreover, the particles are assumed to be monodisperse and of spherical shape.

NUMERICAL DESCRIPTION OF PARTICLES

Two different approaches for the description of the particles are taken. In the first approach we assume that the particles have a characteristic time scale much shorter than typical time scales of the flow, i.e. a very

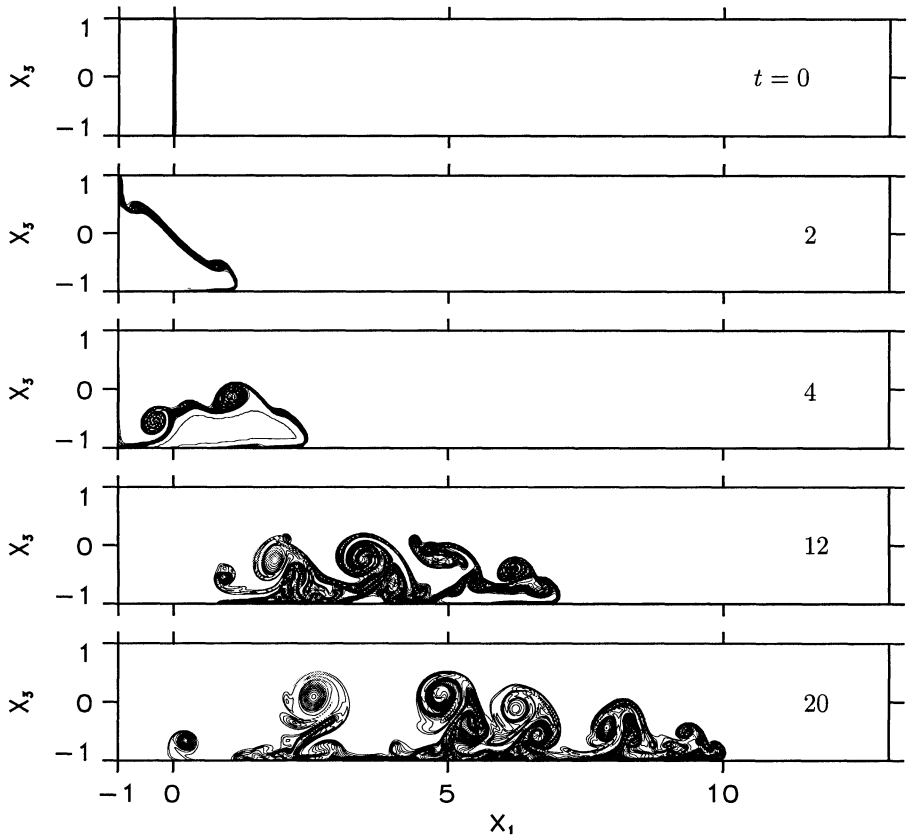

Figure 1: Particle-driven lock-exchange flow at a Grashof number of $2 \cdot 10^7$ (in x_1 only half of the flow domain is shown). Flow visualized by isocontours of the instantaneous particle concentration at different times of the simulation.

small Stokes number $St{=}d_p^2 \rho_p u_b/(18\mu h)$, where d_p and ρ_p are the diameter and density of the particles, respectively, and μ is the viscosity of the fluid. The particle velocity then is identical to the fluid velocity plus a constant settling speed (Maxey, 1987) which can be derived from a balance of the gravitational force and the viscous Stokesian drag of a single free-falling sphere. The particle concentration field is treated in a Eulerian manner in this approach and its temporal evolution is described by a transport equation which also accounts for hydrodynamic diffusion effects (see Davis and Hassen, 1988). The discretization used for this evolution equation corresponds to that employed for the velocity field.

In the second approach particle inertia is taken into account which allows to examine particles with larger characteristic time scales (i.e. finite Stokes numbers). In this case no continuous equation is solved, but a large number of particles are individually tracked in a Lagrangian fashion. We employ a simplified version of the equation for the particle motion given by Maxey and Riley (1983), retaining only the viscous drag and the gravitational force due to density differences which are dominant for our application (for a discussion of the relative importance of forces acting on suspended particles see Lázaro and Lasheras, 1989; Pan and Banerjee, 1996). As pointed out before, the influence of the particles on the fluid phase is modeled by adding a source term on the right hand side of the momentum equations for the fluid. Since in our case the only cause for the fluid motion is the presence of a heavier particulate phase, a two-way coupling between fluid and particles is of course essential. Each of the individually tracked numerical particles represents a cloud of physical particles, and its range of influence extends over several neighboring grid points. The shape function of the particle force is a Gaussian curve of width σ which typically is of the order of the mesh spacing. The initial distance between the particles in the suspension we chose to be at most $\sigma/2$. To solve the particle equations the fluid velocities at the particle locations are needed which are obtained from the velocities at the mesh points by forth-order accurate Lagrangian interpolation (see Martin and Meiburg, 1994). More details

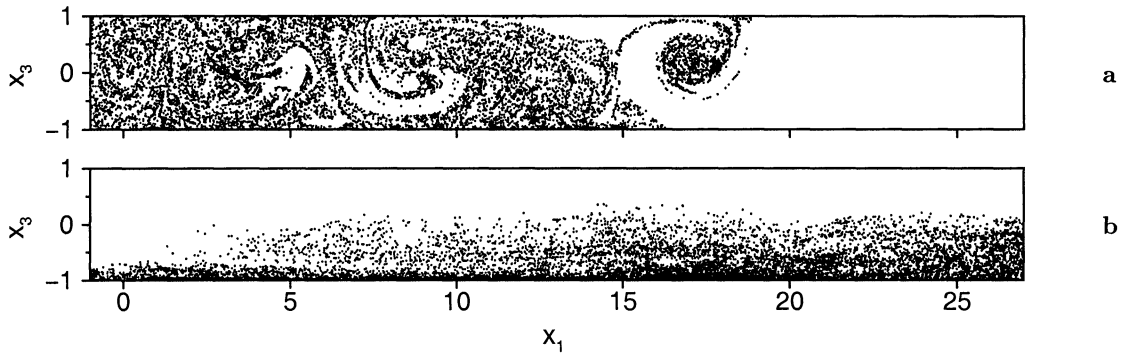

Figure 2: Distribution of passive markers in lock-exchange flows with $Gr=2 \cdot 10^7$ in a channel of finite length (initial configuration as in Fig. 1). Shown are results for a very late stage of the simulation (t=500), when the flow has almost come to rest. **a:** particle-driven gravity current. **b:** density-driven gravity current.

on the basic equations, and the specifics of the numerical implementation will be summarized in a separate publication that is currently being prepared.

RESULTS FOR EULERIAN APPROACH

In Fig. 1 the temporal evolution of a lock-exchange flow is illustrated by means of isocontours of the instantaneous particle concentration field. The Grashof number of the flow is $2 \cdot 10^7$ and the particles have a dimensionless settling velocity of 0.02 (non-dimensionalized by u_b). At time t=0 the suspension, i.e. the particle-laden fluid, is confined to a small portion of the channel on the left. To enable a direct comparison between simulations and laboratory results, this initial set-up is similar to the one used in the experiments of Bonnecaze *et al.* (1993). For t>0 a flow develops which is characterized by two fronts that travel in opposite directions. Between t=2 and 4, the light front in the upper channel half encounters the left boundary and is reflected, which leads to a strong downward motion. At later times, when the flow is increasingly affected by the settling and sedimentation of particles, the pronounced head of the right-propagating front gradually disappears and the horizontal propagation speed decreases. In consequence, the front comes to rest before it encounters the right wall of the channel located at x_1=27. Also, it is seen that the Kelvin-Helmholtz-like billows at the interface develop into a system of dipolar vortices that tend to travel upward. This vertical motion leads to intense mixing of the fluid across the full channel height which becomes obvious from Fig. 2a where the distribution of passive markers is shown at a very late time of the simulation. The markers were added to the particle-laden fluid at time t=0 and indicate the dispersion of the interstitial fluid during the flow development. For comparison, Fig. 2b shows the corresponding distribution of markers that were added to the heavier fluid in a density-driven lock-exchange flow (see e.g. Rottman and Simpson, 1983). Here they are seen to collect in the lower half of the channel. The reason is that in this case the vertical mixing is strongly damped in the late stages of the flow when a stably stratified situation of heavy fluid beneath light fluid has developed.

More detailed insight into the dynamics of the flow shown in Fig. 1 can be gained from the temporal development of the integrated potential and kinetic energy which is depicted in Fig. 3. Also, the time integral of total viscous dissipation is included in this figure. A rapid transformation of potential energy into kinetic energy is seen during the start-up phase, when the flow is strongly accelerated and viscous dissipation is still weak. In the late flow stages, however, this process can be partly reversed, and a certain amount of particles may remain suspended for rather long times. For t>100, say, when only a small fraction of the initial particles are still left in the fluid, the flow develops into an equilibrium state, in which the increase in viscous dissipation equals the decay in kinetic energy. From Fig. 3 it is clearly seen that the limit value the integrated dissipation approaches for large times remains well below the initial potential energy. It can be estimated from the curve that only 40-50% of the initially available potential energy will be converted into the gravity-current flow, while the remainder is "lost" due to particle settling. It must be kept in mind, however, that the results in Fig. 3 were obtained with a two-dimensional simulation model. To what extent these findings apply to fully three-dimensional flows is currently being examined.

To illustrate the influence of viscous diffusion on the flow, Fig. 4 gives results for the time history of the front position x_F for three simulations with different Grashof numbers. x_F is defined as the foremost point of the pro-

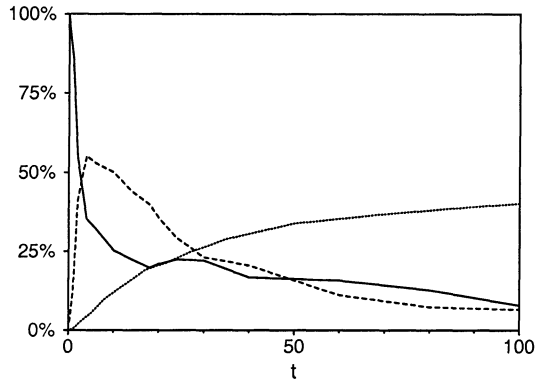

Figure 3: Time history of potential energy (solid line) and kinetic energy (dashed line) integrated over the flow domain (same flow as in Fig. 1). The dotted line gives the amount of energy lost due to viscous dissipation. Results given in per cent of the initial potential energy.

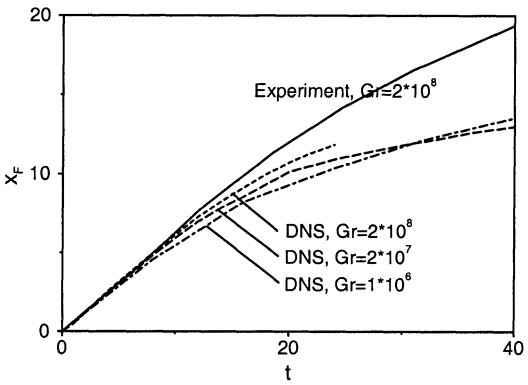

Figure 4: Time history of the front position x_F for three simulations with different Grashof numbers. The flow in Fig. 1 is given by the long-dashed line. Solid line: experimental result of Bonnecaze *et al.* (1993).

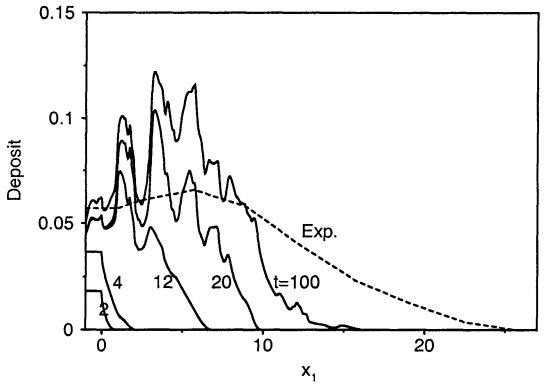

Figure 5: Distribution of particle deposit on the lower boundary (x_3=−1) at different times of the simulation (same flow as in Fig. 1). The dashed line gives the final particle deposit obtained in laboratory experiments conducted by Bonnecaze *et al.* (1993).

pagating current, and is most easily determined from the particle concentration field. Although the settling speed is identical in all cases, it is seen that the fronts spread faster for higher Grashof numbers. This result is to be expected, since for increasing Grashof numbers the retarding forces due to viscous friction in the flow diminish. The crossing of the curves that is seen for the two lower Grashof numbers at about t=30 has probably little significance, since beyond times $t \approx 25$, when most of the particles have already settled out, the front position is not well defined anymore.

Included in Fig. 4 are experimental data of Bonnecaze *et al.* (1993) for the same set-up as used in our simulations, and a Grashof number of $Gr = 2 \cdot 10^8$. At early times when only a few particles have sedimented and the front speed is virtually constant, the corresponding simulation agrees closely with the experimental result. However, after about 10 time units, when the front speed starts to decrease, the curves begin to deviate and the front in the experiment advances more rapidly than in the simulation. The reason for this discrepancy is not fully clarified so far, but we suspect that it can be attributed mainly to the fact that silicon carbide particles were used in the experiment which, in contrast to the numerical particles, are not monodisperse and not of spherical shape. As shown e.g. by Gladstone *et al.* (1998), the presence of only a little amount of smaller particles in the suspension can cause a front to propagate much further than in the case of a strictly monodisperse particulate phase. Also, the assumption of a Stokesian settling velocity may not be justified, if the particles are of strongly non-spherical shape (see Hallermeier, 1981).

Another possible reason for the deviations between experiment and simulation in Fig. 4 is the restriction to a two-dimensional flow in the present simulations. However, for density-driven lock-exchange flows Härtel *et al.* (1999) found that integral parameters like the front speed are very little affected by three-dimensional effects and can accurately be captured by a 2D simulation. We assume that also in the present case 3D effects are not of central importance for the front speed, but we will examine this point in more detail by three-dimensional direct simulations in the next stage of our project.

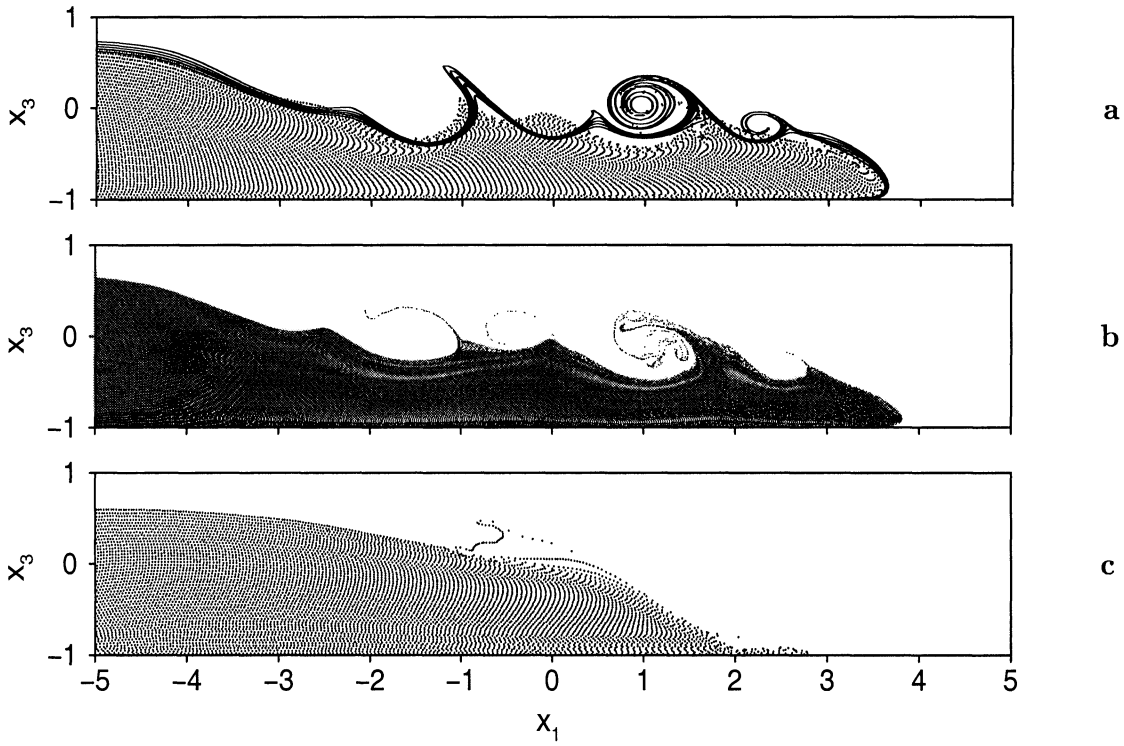

Figure 6: Particle-driven lock-exchange flow simulated with a Lagrangian approach for the particulate phase. Results for different Stokes numbers and different core sizes σ. The settling velocity of the particles and the Grashof number are respectively 0.05 and $2 \cdot 10^7$ in all cases. **a:** $St = 0.01$, $\sigma = 0.1$. The solid lines gives isocontours of the particle concentration of a simulation with a Eulerian particle description. **b:** $St = 0.01$, $\sigma = 0.03$. **c:** $St = 0.1$, $\sigma = 0.1$.

A further comparison of our simulations with the experiments of Bonnecaze *et al.* (1993) is provided in Fig. 5. The curves show the distribution of the dimensionless particle deposit over the channel length at different non-dimensional times, again for the flow shown in Fig. 1. At the latest time (t=100), about 90% of all particles have already settled out. Included in the figure is the experimental sedimentation profile of Bonnecaze *et al.* for a flow with an identical dimensionless settling velocity, but a slightly higher Grashof number. Both experiment and simulation consistently show a weak increase of the particle deposit with x_1, followed by a rapid decay for larger distances from the left boundary. However, in the simulation the particles settle out faster than in the experiment which may indicate that in the experiments a significant resuspension of particles from the bottom wall back into the fluid takes place. This effect is not yet accounted for in our present simulations.

RESULTS FOR LAGRANGIAN APPROACH

For the study of gravity currents driven by very small particles a Eulerian approach for the description of the particulate phase is most efficient. However, if one considers particles with larger Stokes numbers (St>0.01, say), inertia effects need to be taken into account in the description of the particle motion, and a Lagrangian tracking technique must be employed. The potentially strong effect of changes in the Stokes number on the flow structure is illustrated in Fig. 6, where results are given for particles with a dimensionless settling velocity of 0.05 and Stokes numbers of 0.01 and 0.1. In contrast to the cases discussed previously, the interface between clear and particle-laden fluid was located in the middle of the channel in these simulations, which avoids an early reflection of the left-propagating front at the boundary. Concerning the particle effect on the fluid phase, it should be mentioned that we supplement near-boundary particles with their mirror images in order to avoid a spurious gradient in the particle concentration field in the vicinity of the boundaries. We found this to be essential to obtain accurate results, since neglecting the mirror images results in a front speed which is too low by about 5% in our case.

It is seen from Fig. 6 that for a Stokes number of 0.01 the particles still follow the fluid motion closely and the fine-scale vortical structures that develop at the interface can be found from the particle field. For comparison, we have included in Fig. 6a results from a simulation with a Eulerian description of the particle concentration field for the same dimensionless settling velocity. Only small differences can be seen between this simulation and the Lagrangian approach, demonstrating that inertia effects are not yet substantial at Stokes numbers of 0.01. The situation is radically different, though, for Stokes numbers of the order of 0.1 (Fig. 6c). In this case the particles can no longer follow the rapid changes in flow speed at the foremost part and the interface, but settle out continuously while traveling slowly downstream. As a consequence, a distinct front no longer develops.

In the Lagrangian approach one needs to specify the core size σ of the numerical particles, i.e. the width of the region over which the influence of an individual numerical particle and the associated source term are distributed on the computational mesh. In general, a lower limit to σ is set by the mesh size Δ, since particles with a diameter smaller than Δ will "disappear" on the computational grid, if they are located in the center of a mesh cell. On the other hand, it is necessary that the core size of the particles is large enough to make sure that within the suspension the influence regions of neighboring paricles overlap; otherwise the resulting particle concentration field is not sufficiently smooth. This makes clear that the minimum number of particles used, and thus the computational expense, depends directly on the core size of the particles. From our simulations we found that the value of σ may have a discernible influence on the flow evolution. This is illustrated in Figs. 6a and 6b where results are depicted for simulations with different core sizes of the computational particles. In Fig. 6a the core size is 0.1 times the channel half height, while in 6b computational particles with a width of 0.03 were employed. In the latter case a much more detailed resolution of the interface is achieved and it is also seen that the front spreads slightly faster in this case. These results suggest that distributing the particle force over several grid points acts similar to hydrodynamic diffusion in the particle concentration field (note, however, that we have not implemented an explict diffusion term in the particle equation). A careful analysis of the influence of the core size and its relation to the numerical mesh size is an important issue, and we will address this point in more detail in the next stage of our research project.

REFERENCES

Bonnecaze, R. T., Huppert, H. E. and Lister, J. R., 1993, "Particle-driven gravity currents," *J. Fluid Mech.,* Vol. 250, pp. 339-369.

Davis, R. H. and Hassen, M. A., 1988, "Spreading of the interface at the top of a slightly polydisperse sedimenting suspension," *J. Fluid Mech.,* Vol. 196, pp. 107-134.

Gladstone, C., Phillips, J. C. and Sparks, R. S. J., 1998, "Experiments on bidisperse, constant-volume gravity currents: propagation and sediment deposition," *Sedimentology,* Vol. 45, pp. 833-843.

Härtel, C., Kleiser, L., Michaud, M. and Stein, C. F., 1997, "A direct numerical simulation approach to the study of intrusion fronts," *J. Eng. Math.,* Vol. 32, pp. 103-120.

Härtel, C., Meiburg, E. and Necker, F., 1999, "Direct numerical simulation of lock-release gravity currents," subm. to *J. Fluid Mech.*

Hallermeier, R. J., 1981, "Terminal settling velocity of commonly occurring sand grains," *Sedimentology,* Vol. 28, pp. 859-865.

Lázaro, B. J. and Lasheras, J. C., 1989, "Particle dispersion in a turbulent, plane, free shear layer," *Phys. Fluids A,* Vol. 1, pp. 1035-1044.

Martin, J. E. and Meiburg, E., 1994, "The accumulation and dispersion of heavy particles in forced two-dimensional mixing layers. I. The fundamental and subharmonic cases," *Phys. Fluids,* Vol. 6, pp. 1116-1132.

Maxey, M. R. and Riley, J. J., 1983, "Equations of motion for a small rigid sphere in a nonuniform flow," *Phys. Fluids,* Vol. 26(4), pp. 883-888.

Maxey, M. R., 1987, "The gravitational settling of aerosol particles in homogeneous turbulence and random flow fields," *J. Fluid Mech.,* Vol. 174, pp. 441-465.

Pan, Y. and Banerjee, S., 1996, "Numerical simulation of particle interactions with wall turbulence," *Phys. Fluids,* Vol. 8, pp. 2733-2755.

Rottman, J. W. and Simpson, J. E., 1983, "Gravity currents produced by instantaneous releases of a heavy fluid in a rectangular channel," *J. Fluid Mech.,* Vol. 135, pp. 95-110.

Simpson, J. E., 1997, *"Gravity Currents in the Environment and the Laboratory,"* 2nd edition, Cambridge University Press, Cambridge.